

Bicomponent fibre mats with adhesive ultra-hydrophobicity tailored with cellulose derivatives

Laura Taajamaa,^a Eero Kontturi,^{*a} Janne Laine^a and Orlando J. Rojas^{*ab}

Received 30th January 2012, Accepted 10th April 2012

DOI: 10.1039/c2jm30572k

Morphologies featured in bicomponent 2D ultrathin films were reproduced on 3D non-woven microfibre structures. Fibre networks were constructed by electrospinning hydrophobised cellulose derivatives, trimethylsilyl cellulose (TMSC) and cellulose triacetate (CTA), dissolved in a common solvent. Diverse morphologies were obtained depending on the polymer blend ratio: electrospinning of TMSC produced non-continuous micron fibres with shallow dints, TMSC/CTA 5 : 1 flat micron fibres with regular pore arrays, TMSC/CTA 1 : 1 wrinkled micron fibres decorated with shallow dints and occasional larger pores, TMSC/CTA 1 : 5 flat micron fibres with ellipsoidal porous structures and finally, CTA that led to smooth micron and submicron fibres. The fibre mats were ultra-hydrophobic with characteristic water contact angles of *ca.* 150 degrees. In addition, they were characterised by high contact angle hysteresis, and water droplets adhered to the substrate even after tilting the system upside down. Through conversion of the respective components to cellulose, chemical and adsorption properties of the fibre networks could be tuned without significantly altering the large-scale network morphology.

Introduction

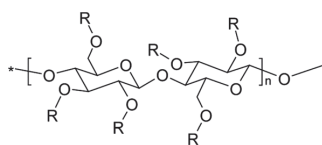
Functional systems with high surface-to-volume and aspect ratios are important drivers in nanoscience. One of the popular means to generate such systems is electrospinning. Electrospinning has been studied for a hundred years,^{1,2} but it received wider attention with the advent of nanotechnology in the 1990s.^{3,4} Nowadays it is a well-established and relatively straightforward method to produce both nano- and micron-scale fibre networks that have found use in applications such as water purification and others involving the control of wetting, fouling and adsorption.⁵⁻⁷ Such interest stems from the fact that distinctive properties emerge when fibres of small diameters are assembled in nonwoven mats.⁵ Hitherto, electrospinning of porous, high surface area fibres has been achieved by utilising highly volatile solvents,⁸⁻¹⁰ coaxial spinning¹¹ and cryogenic liquids.¹² However, the chemical tuning of the fibres obtained with the aforementioned methods is often limited. Therefore, in this work, we introduce bicomponent cellulose derivative systems that can easily and selectively be converted to cellulose and/or dissolved after the fibre formation to tailor the chemical composition and surface and wetting properties of the system.

In our recent report, we discussed the development of ultrathin (<100 nm thickness) bicomponent cellulose derivative films with phase-specific pore formation.¹³ These films were constructed by spin coating mixtures of trimethylsilyl cellulose (TMSC) and cellulose triacetate (CTA). The formation of the observed morphologies was ascribed to complex phenomena occurring upon spin coating, including vertical and lateral phase separations according to the transient bilayer theory, plasticization of the CTA phase under a humid atmosphere leading to dewetting and phase-specific pore growth and, finally, surface energy minimization resulting in partial layer inversion during dewetting. We speculated on the possibilities of translating the obtained unique morphologies into higher level systems, for example, fibre networks. Thus electrospinning, a non-equilibrium, kinetically controlled process with a characteristic time scale comparable to that of spin coating (10^{-3} to 10^{-4} s range), was used to produce microfibers with the same precursor polymer blends. In electrospinning, a high voltage induces a polymer jet when an electric field at the tip of a spinneret overcomes the surface tension of the polymer solution. As the charged liquid jet bends, elongates and travels in a longitudinal electric field towards a ground collector, the solvent evaporates and a non-woven fibre network is formed.^{3,7}

In principle, almost all soluble polymers can be electrospun into fibre networks and hitherto many biopolymers have successfully been used as such or in multiphase systems.^{5,14} Cellulose (Chart 1) is the most abundant biopolymer and has recently caught increased attention as a source for nanomaterials

^aDepartment of Forest Products Technology, School of Chemical Technology, Aalto University, P. O. Box 16300, FI-00076 Aalto, Finland. E-mail: eero.kontturi@aalto.fi; o Rojas@ncsu.edu

^bDepartment of Forest Biomaterials, North Carolina State University, Box 8005, Raleigh, North Carolina 27695-8005, USA



Cellulose R=H
Trimethylsilyl cellulose R=Si(CH₃)₃
Cellulose triacetate R=COCH₃

Chart 1 Chemical structures of cellulose, TMSC and CTA.

with, for example, unusual strength and liquid crystalline characteristics.¹⁵ However, the poor solubility of cellulose in common organic solvents limits its electrospinnability. For this reason, readily soluble cellulose derivatives, especially cellulose acetates, have been utilised with success.^{14,16} Furthermore, electrospinning of cellulose fibres from direct, often exotic solvents has been demonstrated.^{17–20} Typical solvents for cellulose are multicomponent mixtures, which often include salts and have a low vapour pressure; therefore, coagulation baths (for salt removal) and heated collectors (for solvent removal) are used to prevent fibre fusion.¹⁶ Because such regeneration systems are often complex and laborious, micro- or nanocellulosic objects have also been obtained by energy-intensive top-down breakdown of the native structures.¹⁵ By contrast, here the construction of related networks is proposed by using a facile bottom-up method by electrospinning solutions of bicomponent cellulose derivatives. The two hydrophobised polysaccharides exploited are TMSC and CTA (Chart 1). Regeneration to cellulose from TMSC²¹ or CTA²² as well as surface-selective conversion of CTA²³ has been reported.

Surface functionalization of cellulosic materials is often complex^{24,25} and therefore, the purpose of this work is to introduce a simple method to prepare cellulose fibre mats with tunable chemical and adsorption characteristics. Additional motivation is provided by the peculiar properties inherent to the biopolymers used. More generally, utilisation of polysaccharides that are renewable, non-toxic and biodegradable promotes sustainability and offers a step towards greener materials in chemistry and engineering.

Experimental

Materials

TMSC was obtained from Thuringian Institute of Textile and Plastics Research and CTA from Fluka. According to the manufacturers, the degree of substitution (DS) of TMSC was 2.8 and the acetyl content of CTA was 43–49 wt% (corresponding to DS ~3). All solvents and other chemicals were of analytical grade and used as obtained.

TMSC and CTA stock solutions (100 g dm⁻³) were prepared by dissolving the polymers in chloroform. The stock solutions were allowed to stabilise overnight and mixed to obtain given TMSC/CTA weight ratios for a total polymer concentration of 100 g dm⁻³. The pure CTA fibre networks were prepared from a 50 g dm⁻³ solution.

Electrospinning

Fibres from TMSC/CTA solutions were obtained by horizontal electrospinning. The setup consisted of a computer-controlled syringe pump (Aldrich) to inject the polymer solution through a needle ($d = 1.37$ mm) connected to the positive terminal of a high-voltage supply unit (Series EL, Glassman High Voltage). A metal plate ($d = 30$ cm) covered with aluminium foil was used as a collector connected to the negative electrode of the power supply (ground). The electrospinning parameters were selected by performing a series of runs with different polymer concentrations, flow rates, electric field strengths and tip-to-collector distances. The parameters were chosen to obtain the best possible fibres and to reduce the amount of defects like beading (Table 1).

Selective conversion and dissolution

All possible modifications of TMSC and CTA components (conversion or dissolution) after the fibres were produced are depicted in Scheme 1. The first level is selective conversion: either of the two cellulose derivatives can be converted to cellulose (to obtain “TMSC/Cellulose” or “Cellulose/CTA”). The second level involves two possible paths: (i) conversion of the remaining cellulose derivative to cellulose (producing “Cellulose/Cellulose” fibres) or, (ii) selectively dissolving it with chloroform (producing “Cellulose/-” or “-/Cellulose” fibres). These modifications were applied to various polymer blends; however, the TMSC/CTA 5 : 1 fibre networks were used here to illustrate the matrix of conditions shown in Scheme 1 (see Fig. 6 and the respective discussion in other sections of this paper).

TMSC was converted to cellulose by hydrolysing the electrospun fibre mats in vapour from 2 M HCl solution under vacuum for 2 minutes.²¹ The full conversion of CTA to cellulose was performed by exposing the fibre mats to an aqueous ammonia vapour environment for 11 days.²²

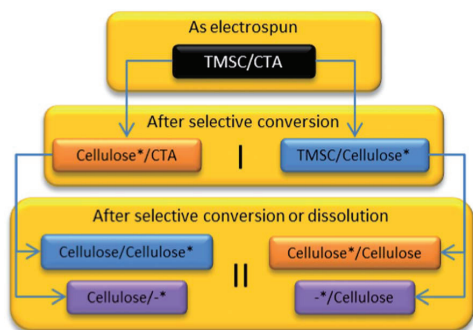
Since cellulose does not dissolve in common organic solvents it was possible to dissolve the non-converted cellulose derivative in chloroform after the selective conversion of either of the components. The dissolution was performed by immersing the fibre mats in excess chloroform for 1 h with occasional stirring followed by rinsing with ~50 ml fresh chloroform.

Attenuated total reflectance infrared spectroscopy (ATR-IR)

A Bio-Rad FTS 6000 spectrometer (Cambridge, MA, USA) was used to scan the 4000–700 cm⁻¹ region at a constant mirror velocity of 20 Hz, 5 kHz filter, and 8 cm⁻¹ resolution. Air background spectra were acquired before each set of

Table 1 Electrospinning parameters. The tip-to-collector distance was 10 cm and all the fibre mats were produced at room temperature and at ambient humidity

TMSC/CTA blend ratio (w/w)	Voltage, kV	Flow rate, cm ³ h ⁻¹
1 : 0	20	5
5 : 1	20	5
1 : 1	12.5	2
1 : 5	10	2
0 : 1	15	2



Scheme 1 Possible modification pathways for TMSC/CTA bicomponent fibre mats. The first level (I) indicates two possible modification routes: conversion of TMSC or CTA to cellulose. The second level (II) includes two possible modification routes: selective dissolution or conversion of the remaining component. The altered component is marked with an asterisk.

measurements. For each measurement a minimum of 200 scans per spectrum were collected, ATR-corrected and normalised at 1300 cm^{-1} . The spectra shown throughout this article are averages of at least three measurements from various points of the fibre network.

Field emission scanning electron microscopy (FE-SEM)

The fibre network and fibre surface morphology were studied using a JSM-6400F instrument (JEOL Ltd., Tokyo, Japan) operated at an accelerating voltage of 5 kV and a working distance of 20 mm. Prior to imaging, a $5 \times 5\text{ mm}$ piece of the mat was fixed on conductive carbon tape, mounted on the support and then sputtered with a *ca.* 6 nm layer of gold/palladium (Au/Pd).

Contact angle (CA)

The water contact angles were measured to investigate the hydrophobicity/hydrophilicity of the fibre networks. A CAM-200 contact angle goniometer (KSV Instruments Ltd, Helsinki, Finland) was used. Contact angle calculations were performed with the software provided by the goniometer manufacturer and they are based on a numerical solution of the full Young–Laplace equation. The measurements were conducted in ambient air at room temperature. The reported static and dynamic contact angles are the averages of the respective measured duplicate samples prepared using the same conditions. Each sample was used in multiple measurements to obtain a representative value. The errors represented are standard deviations.

Static equilibrium contact angles were determined at the three-phase line when stable values were observed (less than ten seconds after drop deposition). The water droplet volume was $6.7\text{ }\mu\text{L}$. The advancing and receding dynamic contact angles were obtained by increasing and decreasing ($0.1\text{ }\mu\text{L s}^{-1}$) the volume of a small water droplet (originally $5\text{ }\mu\text{L}$) with a thin needle. The typical fibre mat area occupied by the water drop at maximum drop volume (*ca.* $44\text{ }\mu\text{L}$) was approximately 50 mm^2 . At least three reproducible measurements from duplicate samples were performed.

Nitrogen adsorption–desorption measurements

The specific surface area was determined by N_2 adsorption with Omnisorp 100CX (Coulter, Miami, FL, USA) at the temperature of liquid nitrogen. Prior to measurements, the sample was dried at $100\text{ }^\circ\text{C}$ for 10 hours. Both adsorption and desorption isotherms were measured and the surface area was determined from the adsorption curve by the Brunauer–Emmet–Teller (BET) method. In addition to micro- ($<2\text{ nm}$) and mesopores ($2\text{--}50\text{ nm}$), nitrogen adsorption is able to detect a fraction of the macropores ($>50\text{ nm}$). Therefore, a small number of pores between the fibres can also fall into the measurement range of the nitrogen adsorption but their contribution is negligible when compared with the copious amount of pores on the fibre surface.

Other methods

Differential scanning calorimetry (DSC) measurements were conducted with DSC Q100 (TA Instruments, New Castle, DE, USA). The heating–cooling circle from 25 to $250\text{ }^\circ\text{C}$ was repeated twice using a heating rate of $10\text{ }^\circ\text{C min}^{-1}$. A confocal Leica DMRXE microscope (Leica Microsystems GmbH, Mannheim, Germany) was utilised in roughness analysis. The roughness was determined from $750 \times 750\text{ }\mu\text{m}^2$ images obtained from several points of the sample.

Results and discussion

Typical SEM images of the TMSC/CTA electrospun fibre mats are shown in Fig. 1. The overall structure of the fibre network is presented (Fig. 1, top row) together with a more detailed image depicting the morphology of the fibre surface (Fig. 1, middle row). Pure TMSC (TMSC/CTA 1 : 0) and CTA (TMSC/CTA 0 : 1) fibres were rather smooth. The thinnest and the most uniform fibres were produced from pure CTA although some beading occurred. Shallow dints with diameters up to 40 nanometres were observed on the surface of TMSC fibres. Regular dints in the range of a hundred nanometres have been reported to arise from the use of highly volatile solvents, such as dichloromethane.⁹ The porous structure arose from rapid phase separation during electrospinning after the solvent-rich regions were replaced with an array of dints. Bognitzki *et al.* observed that the tendency of PLLA fibres to form dints was reduced when a solvent with a lower vapour pressure, *e.g.*, chloroform was used.⁹ TMSC produced discontinuous fibres; however, when some CTA was added to the electrospinning solution, a continuous fibre network emerged (TMSC/CTA 5 : 1). A similar phenomenon was reported by Qi and co-workers, however, with cellulose dissolved in an aqueous NaOH/urea solvent. With this solvent system, they were only able to obtain continuous fibres by blending cellulose with polyol binders.²⁶

The TMSC/CTA bicomponent fibres were flat, ribbon- or sheet-like and some twisting, wrinkling and beading occurred. The formation of beads has been ascribed to axis-symmetric jet instability, *i.e.*, Rayleigh instability mode which is an axis-symmetric extension of the classical Rayleigh instability when electrical effects are important: instead of the thinning effect caused by asymmetrical whipping, the jet fluctuates evenly around its main axis.²⁷ The surface morphology of bicomponent fibres, especially TMSC/CTA 5 : 1 and 1 : 5, was porous.

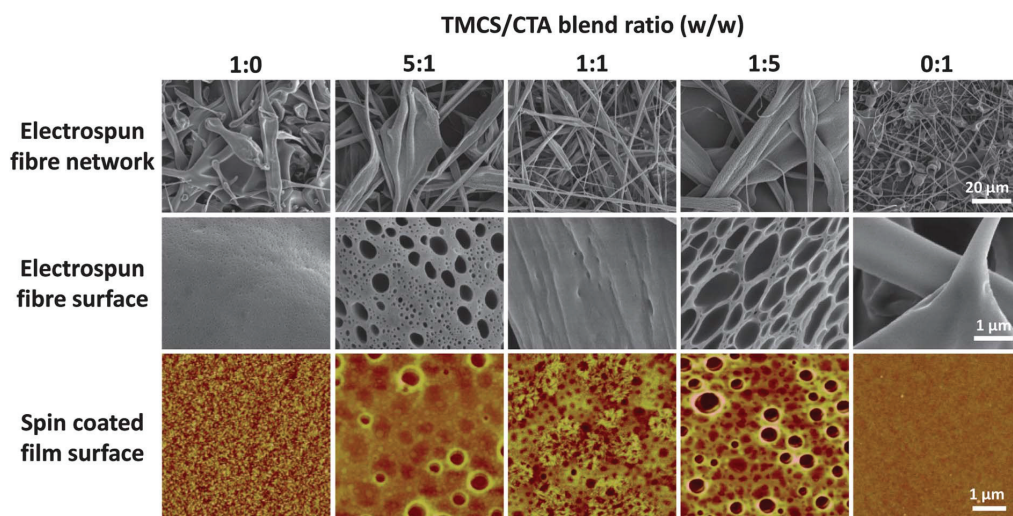


Fig. 1 FE-SEM images of TMSC/CTA bicomponent fibre mats (top) and respective fibre surfaces (middle). AFM height images of solid, ultrathin TMSC/CTA bicomponent film surfaces (bottom) are included as a reference. The TMSC/CTA blend ratios are indicated at the top and scale bars are on the right.

During electrospinning, the surface area of the fibre increases significantly as the solvent evaporates during the process time scale of milliseconds. With bicomponent systems, this could lead to various thermodynamically driven consequences, *e.g.*, crossing the phase boundaries leading to phase separation. Phase separation can be triggered by various means and typically it is achieved *via* vapour or temperature annealing.⁸ Phase separation *via* spinodal decomposition occurs due to the growth of unstable concentration fluctuations, as has also been proposed for porous fibre morphologies.⁹ In addition, high relative humidity during electrospinning can induce pore formation, for example, by generating the so-called breath figures.⁸ Breath figures are formed when the evaporation of a high vapour-pressure solvent leads to cooling of the surface, which in turn enables the condensation of water from the ambient air.²⁸ Several groups have studied the effect of humidity on electrospinning.^{8,9,29,30} Casper and co-workers concluded that breath figure formation alone is not sufficient to fully explain the complex morphology changes that occur during electrospinning.²⁹

In the TMSC/CTA 1 : 5 fibre network, the pores were elongated along the fibre axis, *i.e.*, they were ellipsoidal in shape. Bognitzki *et al.* have reported that ellipsoidal pores are a result of a uniaxial extension of the jet.⁹ The pores in fibres from TMSC/CTA 5 : 1 were more circular and regular. This porous structure was studied further with BET nitrogen adsorption: a surface area and a total pore volume of 25 m² g⁻¹ and 0.053 cm³ g⁻¹ were measured, respectively. The average pore diameter was 83 Å for pores smaller than 371 nm. Fibres from electrospun synthetic polymers, such as polycarbonate, poly(ethylene oxide) and poly(methyl methacrylate), can reach extremely high surface areas of 100–1000 m² g⁻¹.⁸ However, the present results either exceed or are in line with those reported for porous electrospun cellulose acetate fibres (surface areas of 13.7–14.5 m² g⁻¹)³¹ and

nanofibrillar cellulose aerogels (15–70 m² g⁻¹).^{32,33} As a reference, we note that cellulose nanofibrils disintegrated from wood with a diameter of 3–5 nm correspond to a theoretical specific surface area of approximately 600 m² g⁻¹.³⁴

As a reference, Fig. 1 (bottom row) shows atomic force microscopy (AFM) height images of ultrathin films obtained after spin coating TMSC, CTA and their mixtures from chloroform. This enables a comparison between 3D fibre network surfaces and the 2D flat films to be made. Films with pure polymer or bicomponent films with an excess of the other component were smooth and featureless. TMSC films were coarser compared to CTA films. In films with TMSC and CTA blend ratios of 5 : 1 to 1 : 5 micron scale pore growth was observed. Increasing the amount of CTA in the blend enhanced the pore growth in the fibres. In addition, increasing the CTA fraction in the electrospinning solution increased the pore size. Systems with equal amounts of TMSC and CTA (TMSC/CTA 1 : 1) led to fibres with reduced pore growth. The fact that the results described above are largely congruent with our previous study on thin solid films is noteworthy.¹³

The fibre dimensions estimated from the SEM images are shown in Table 2. Two values are given in cases where a bimodal fibre width distribution was measured. The seemingly simple electrospinning process results from a complex combination of process variables, including strength of the electric field and solution pumping rate. Likewise, the fibre morphology and dimensions depend mainly on the nature of the polymers (molecular weight and distribution, glass transition temperature and solubility), polymer solution (viscosity, surface tension and conductivity), solvent (vapour pressure), substrate and relative humidity.⁵ It has been reported that with careful optimisation of the polymer blend and spinning parameters, the fibre diameter can be tailored within a broad range and even down to some tens of nanometres.³⁵

Table 2 Fibre dimensions estimated from the SEM images

TMSC/CTA blend ratio (w/w)	Fibre width, μm	Bead diameter, μm	Pore diameter, μm	Dirt diameter, nm
1 : 0	0.4–10	<70	—	40
5 : 1	2–10	<70	<0.6, <0.1	100
1 : 1	0.4–2	<40	—	<60, <600
1 : 5	2–10	<70	<0.1 and <1.6 ^b	100, 200
0 : 1	0.4–1 ^a	<40	—	—

^a Fibre diameter. ^b The elongated diameter (*i.e.* the longest side to side diameter of the elongated pore).

ATR-FTIR spectra of the TMSC/CTA fibre mats in the double bond and finger print regions ($1900\text{--}500\text{ cm}^{-1}$ wavenumber range) are presented in Fig. 2. Trimethylsilyl groups, abundant in TMSC but not present in cellulose or CTA, are distinguishable markers.

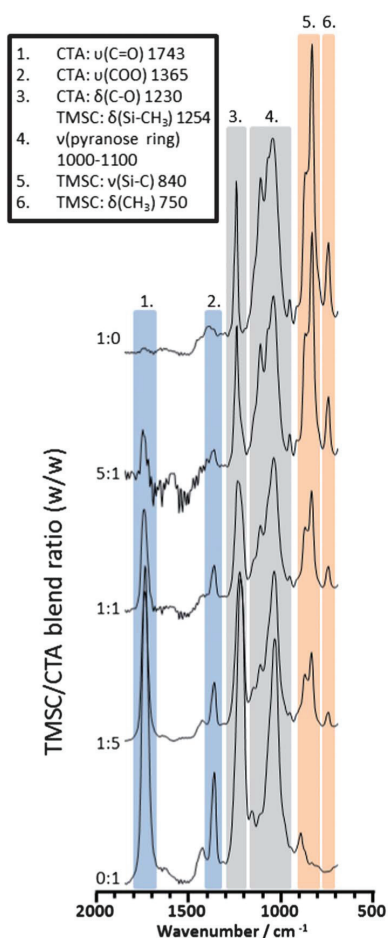


Fig. 2 ATR-FTIR spectra ($1900\text{--}700\text{ cm}^{-1}$ wavenumber range) of the TMSC/CTA fibre mats. The blend ratios are stated on the left and the characteristic peaks for TMSC and CTA are indicated in the legend.

Characteristic peaks for TMSC in the range presented in Fig. 2 are Si-CH₃ bending at 1254 cm^{-1} and Si-C stretching at 840 cm^{-1} . CH₃ bending at 750 cm^{-1} increased as the amount of trimethylsilyl groups increased. Characteristic features for CTA are C=O stretching at 1743 cm^{-1} , COO stretching at 1365 cm^{-1} and C-O bending at 1230 cm^{-1} . Pyranose ring stretching is visible between 1100 and 1000 cm^{-1} . It can be concluded that the chemical composition of the fibre networks followed the expected chemical composition of the bicomponent polymer solutions: the more TMSC in the polymer solution, thus also in the fibre network, the stronger was the contribution from the characteristic peaks of TMSC. The same is naturally valid for CTA.

Water contact angle (WCA) measurements provide information on the topmost molecular layer. TMSC is hydrophobic while CTA and cellulose are hydrophilic materials; thus, tunable hydrophobicity is inherent to the TMSC/CTA system. Fig. 3, Table 3 and Fig. 4 summarize WCA data for these systems. The static equilibrium WCAs in the flat bicomponent films were between $93 \pm 1^\circ$ (pure TMSC) and $58 \pm 0.5^\circ$ (pure CTA). The corresponding WCAs for the fibre mats are presented in Fig. 3 and they were in the range between $150 \pm 11^\circ$ (pure TMSC) and $129 \pm 2^\circ$ (pure CTA). A 20 degree WCA decrease was noted in the bicomponent fibre mats, when the TMSC fraction decreased from one to zero. More drastic changes occurred when the TMSC component was converted to cellulose (producing “Cellulose/CTA” fibre mats): the WCAs decreased *ca.* $150\text{--}140$ degrees at all the blend ratios with TMSC as the majority component. Only the bicomponent fibre mat “Cellulose/CTA” 1 : 5 remained at the initial, higher WCA value. Such a high WCA value might be explained by the assumption that there was very little TMSC on the fibre surface. Thus, the regeneration of TMSC into hydrophilic cellulose could not alter the contact angle from that of pure CTA fibres. After CTA conversion to cellulose, the WCA of the pure CTA fibre mat decreased from $129 \pm 2^\circ$ to $31 \pm 5^\circ$. In all the other bicomponent “TMSC/Cellulose” fibre mats, the WCAs decreased only by approximately ten degrees. This indicated that TMSC is probably located as the topmost surface layer.

Table 3 includes the WCAs of electrospun fibre mats and respective ultrathin films (spin coating) of bicomponent (TMSC/CTA) systems. In the ultrathin TMSC/CTA films, a critical, small amount of TMSC brought the WCA to a value close to that

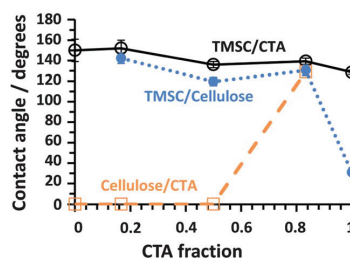


Fig. 3 Static WCA for (i) untreated (○, solid line), (ii) TMSC converted (□, broken line), and (iii) CTA converted (●, dotted line) TMSC/CTA bicomponent fibre mats. The CTA fractions 0, 0.5 and 1% correspond to TMSC/CTA blend ratios 1 : 0, 1 : 1 and 0 : 1, respectively. The lines are added to guide the eye.

Table 3 Comparison of the static WCA of TMSC/CTA bicomponent fibres and ultrathin films. The WCA value of ultrathin films is indicated in parenthesis. The CTA conversion of the films was not studied further

TMSC/CTA blend ratio (w/w)	Fibre contact angle (film contact angle), degrees				
	1 : 0	5 : 1	1 : 1	1 : 5	0 : 1
Untreated (TMSC/CTA)	150 ± 11 (93 ± 0)	152 ± 8 (92 ± 2)	136 ± 3 (92 ± 0)	139 ± 3 (92 ± 1)	129 ± 2 (58 ± 1)
TMSC converted (cellulose/CTA)	0 (59 ± 1)	0 (62 ± 1)	0 (47 ± 1)	129 ± 3 (56 ± 2)	
CTA converted (TMSC/cellulose)		142 ± 2	120 ± 5	130 ± 4	31 ± 5 (13 ± 2)

of pure TMSC and it was concluded that a thin TMSC overlayer was present on the film.¹³ In the present case of electrospun fibre mats, a similar effect was observed. There was also a decrease in WCA with decreasing amount of TMSC in the fibres; however, the change was subtle. Roughness plays a significant role in the contact angle measurements³⁶ and here the effect was noted to be substantial. Fibre mats have typical roughness on multiple length scales and the roughness determined by confocal microscopy was on the micrometre scale. This is approximately thousand-fold larger compared to the smooth spin coated films. The WCAs of pure TMSC and CTA increased respectively from $93 \pm 1^\circ$ and $58 \pm 0.5^\circ$ (smooth films) to $150 \pm 11^\circ$ and $129 \pm 2^\circ$ (rough fibre mats). When the TMSC component was converted to hydrophilic cellulose, the roughness of the fibre mats also emphasised the increase in hydrophilicity. The WCA on smooth films decreased by only 33–39% while the fibre mat WCAs were reduced from *ca.* 150–136° down to zero. Based on the Wenzel equation, the enhancing effect of roughness on the hydrophobicity or hydrophilicity is inherent for Wenzel state surfaces. However, the difference between 2D and 3D systems cannot be attributed to the Wenzel state alone, as could be noted from, *e.g.*, the increase in WCA from 58° to 129° in pure CTA fibre mats.

In addition to WCA, the paraffin oil contact angle was measured to be $74 \pm 14^\circ$ for TMSC/CTA 1 : 5 fibre mats. Korhonen *et al.* have recently demonstrated that super-hydrophobic and oleophilic materials could have potential in environmental applications, *e.g.*, cleaning of oil spills.³⁷ This demonstrates a possible application for the present system: an oil absorbing device that floats on water.

Care needs to be taken when interpreting the contact angle results. Among others, Gao and co-workers argue that the static contact angle is just a random metastable state in between the advancing and receding contact angles and further, that only events at the contact line have an effect.^{38–40} Marmur and Bittoun are of the opinion that local conditions at the contact line determine the actual contact angles and the global, the most stable apparent contact angles.⁴¹ Furthermore, they claim that the Wenzel or Cassie–Baxter equations are applicable when the water drop is sufficiently large compared to the wavelength of the heterogeneity (chemical or topographical) and also large enough to avoid errors due to non-axis-symmetry.^{41,42}

To avoid ambiguity, advancing and receding CA were measured (Fig. 4). Most of the fibre mats tested had an advancing WCA of *ca.* 150 degrees. Contact angle hysteresis (CAH), the difference between advancing and receding contact angles, was used to indicate the propensity of the drop to move on the surface. CAH occurs due to surface heterogeneities, be that chemical or topographical.^{38,43} The measured CAH values

were high, with a minimum of 50 degrees. CTA had the largest CAH, with approximately 140 degrees. Typically, the threshold CAH for slipping has been considered to be 10 degrees, but Cho and Chen have indicated that once the CAH exceeds 45 degrees, the water droplet no longer slides but becomes pinned.⁴⁴ Extrand has claimed that in addition to the reasons mentioned above, an

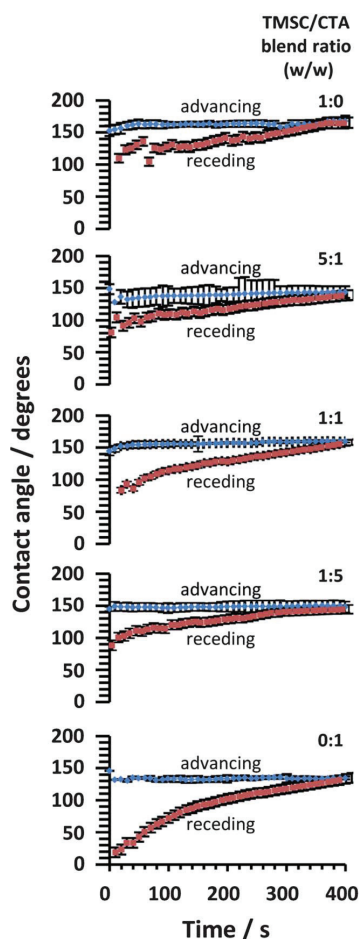


Fig. 4 Dynamic WCAs for untreated TMSC/CTA bicomponent fibre mats. Angles are the average of at least three measurements and two parallel films and the error is the standard deviation. Experimental points were filtered to include only every tenth point for clarity.

inherent hysteresis arising from molecular interactions at the contact line, *i.e.*, the adhesive bond between the liquid and solid, is present on most surfaces.⁴⁵

A study on the wettability of fractal surfaces by Onda *et al.* marked the onset of wider attention on superhydrophobic surfaces⁴⁶ and since then the utilised nomenclature has become more diverse and complex. Roach *et al.* suggested the need to consolidate the terminology used in high contact-angle materials: (i) “positive contact-angle enhancement” should be used if the contact angle is increased by additional roughness but is less than 120 degrees; (ii) “ultrahydrophobicity” is indicated if the contact angle is increased by roughness to values greater than 120 degrees; and (iii) “superhydrophobicity” is when the contact angle is increased to values greater than 150 degrees and the contact-angle hysteresis is less than 10 degrees.⁴⁷ With this terminology in mind, the TMSC/CTA fibre mats can be classified as ultra-hydrophobic.

The behaviour of water droplets on a surface is related to both surface chemistry and morphology.⁴⁶ Conventionally, there are two models to explain contact-angle enhancement on rough homogeneous surfaces, namely Wenzel (homogeneous)³⁶ and Cassie–Baxter (heterogeneous),⁴⁸ but other definitions have also been proposed.⁴⁹ In the Wenzel model, complete liquid penetration into indentations is proposed while in the Cassie–Baxter one, air pockets are suggested to exist below the water drop and inside the indentations.⁵⁰ Surfaces in the Wenzel state are envisaged to be “sticky” or adhesive to the probing liquid whereas in the Cassie–Baxter state the surfaces are described as “slippy”, *i.e.*, the water droplet rolls off easily.^{51,52} The obtained fibre mats of TMSC/CTA were tested for these effects and it was observed that water droplets stay pinned on top of the structure, even when it was turned upside down (Fig. 5). This high-adhesive behaviour seems to indicate a Wenzel-type of system, although other wetting regimes, *e.g.*, Cassie impregnating state, have been proposed.⁴⁹ Similar behaviour was reported by Feng *et al.*: hierarchical micro- and nanostructured morphologies enabled hydrophobicity and at the same time high adhesive force with water.⁵³ They also reported that once the volume of the water droplet is above *ca.* 10 μL , a balance between the weight and the surface tension is exceeded and the water droplet becomes detached.

Even though adhesive ultra-hydrophobicity is a less studied field than, for example the superhydrophobic lotus leaf effect, several accounts on the subject exist.^{44,54–56} Some examples include fluorinated cellulose aerogels,⁵⁴ oxygen plasma etched cellulose paper⁵⁵ and electrospun polymer/silica mixtures.⁵⁶ There are also procedures with alternative steps to obtain either “sticky” or “slippy” surfaces,⁵⁷ and also reversible switchable adhesive properties^{58,59} have been reported. Applications such as lubrication,⁵⁵ printing⁵⁶ and microfluidics,⁵⁷ have been proposed. Guo and Liu stated that adhesive superhydrophobicity was due to the hierarchical surface structures and that capillary and van der Waals forces between the surface and water gave rise to strong adhesion.⁶⁰ Partial filling of the pores,⁶¹ decreased contact line tension, roughness, increased wetted surface fraction⁵⁶ and chemical heterogeneity have also been claimed to cause high adhesion.⁵⁵

Finally, the TMSC/CTA 5 : 1 fibre networks were subjected to modification steps involving regeneration to cellulose as

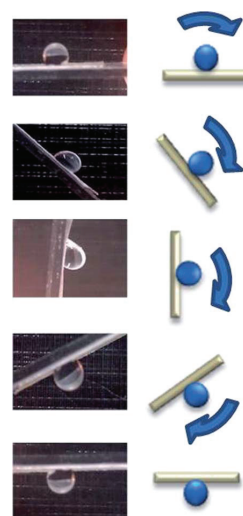


Fig. 5 Photographs of a water droplet pinned on top of a tilted TMSC/CTA 5 : 1 fibre mat.

presented in Scheme 1 and the morphology of the system as well as the WCA are included in Fig. 6. The sample matrix preparation is explained in detail in the Experimental section. The SEM images (Fig. 6, left of each panel) depict the fibre network on a large scale together with the static WCA images. The image on the right of each panel indicates the morphology of the fibre surface (higher SEM magnification).

There were no visible changes in the fibre network morphology on a large scale after any of the modification steps. Minor changes were observed only after closer examination. The pore dimensions appeared somewhat distorted in the two cases with cellulose derivative conversion and sequential dissolution. The surface morphology was mainly unchanged after the modification steps that took place in the vapour phase, *i.e.*, TMSC and CTA conversion into cellulose. However, round, crystal-like structures with diameters up to 1 μm embedded to the polymer matrix were observed after successive TMSC and CTA conversions. These crystals were not soluble in water but they disappeared after treatment with a mild acid. Beneath the crystals the fibre morphology was intact. It is likely that these crystals were ammonium acetate that formed during the conversion of CTA to cellulose; more detailed characterization of these residual crystals is outside the scope of the present discussion.

The ability of this bicomponent system to form a versatile and tailored matrix with uncomplicated modification steps is highlighted in Fig. 6. As mentioned before, the contact angle decreased radically after the TMSC conversion to cellulose. The WCA seemed relatively high in the fibre mat where CTA had been converted to cellulose. The effect of CTA conversion was reduced due to a low amount of CTA in this blend (CTA fraction 0.17). The high contact angle after consecutive CTA conversion and TMSC dissolution could be explained by the fact that during the selective dissolution, there is always some re-adsorption of the solute to the surface.⁶²

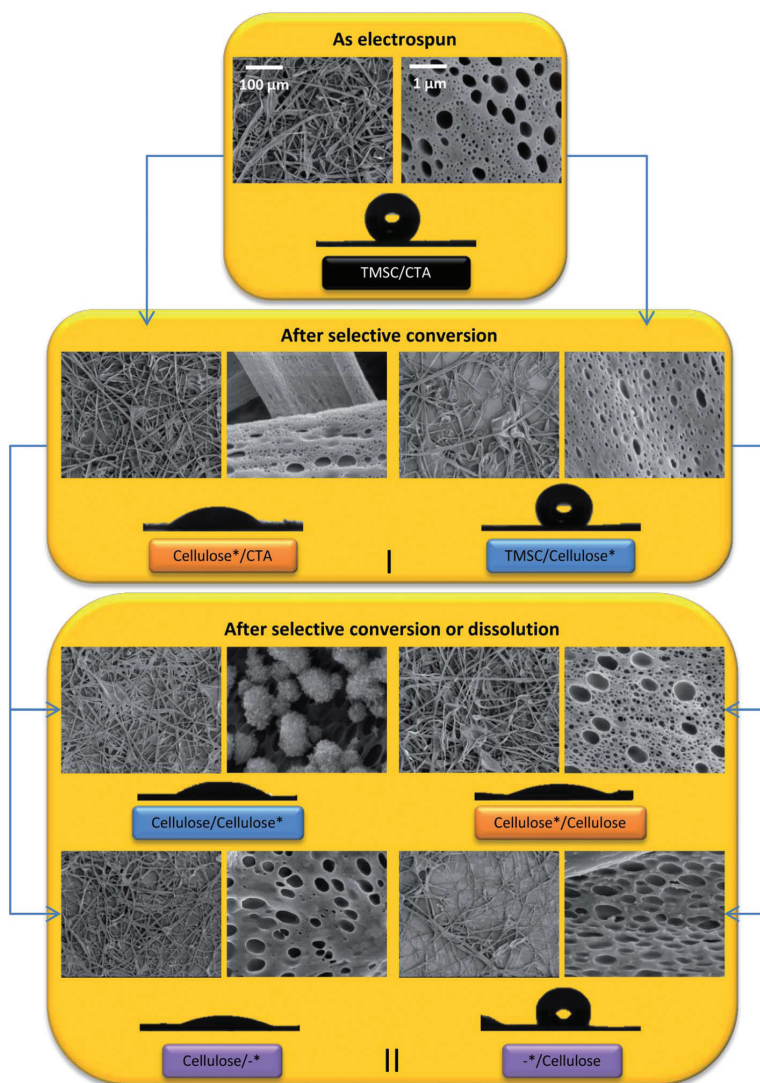


Fig. 6 SEM and static water contact angle images of the TMSC/CTA 5 : 1 modification according to Scheme 1. The first level (I) indicates two possible modification routes: conversion of TMSC or CTA to cellulose. The second level (II) includes two possible modification routes: selective dissolution or conversion of the remaining component. The altered component is marked with an asterisk. The scale bars (100 μm , left and 1 μm , right) from the top row carry on throughout the figure, for each pair of SEM images.

It is possible to gain information on the distribution of the components in an electrospun fibre either by annealing the fibre mat at elevated temperatures or by selectively dissolving one component.¹² The glass transition temperatures of TMSC (193 °C) and CTA (192 °C) were determined by DSC and they were too close to one another to study the component distribution by annealing. In addition to demonstrating the diversity of the possible modification paths, selective dissolution yielded valuable information about the morphology and polymer distribution. Table 4 summarizes the results from the dissolution experiments.

Bognitzki *et al.* have drafted four possible schemes for component distribution in bicomponent fibres: (i) fibres are formed by the individual pure components, (ii) fibres consist of sequences of the pure components or the two components are separated on a scale smaller than fiber diameter and the other component forms either (iii) matrix-dispersed or (iv) co-continuous domains.¹² To summarise the experimental findings, an illustrative schematic diagram of the possible component distribution in the fibres is provided in Scheme 2. Due to the observation that the network was destroyed only when CTA, as the

Table 4 Summary of qualitative description of the fibre mats after selective conversion and dissolution (see Scheme 1 and Fig. 6)

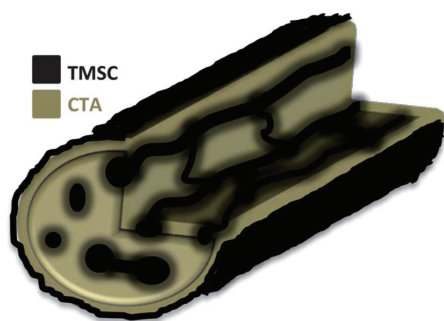
TMSC/CTA blend ratio (w/w)	5 : 1 (TMSC majority)	1 : 5 (CTA majority)
TMSC converted to cellulose and CTA dissolved	Fibre network maintained	Fibre network destroyed
CTA converted to cellulose and TMSC dissolved	Fibre network maintained	Fibre network maintained

majority component, was selectively dissolved (Table 4), it was concluded that CTA formed a continuous matrix. Based on the contact angle measurements (Fig. 3), TMSC formed a layer on top of the fibres. Additionally, TMSC was hypothesised to reside as interconnected domains embedded in the CTA matrix. Interconnected TMSC domains ensured that the integrity of the fibre network remained when CTA component was dissolved as long as it did not form the majority phase (Table 4). Interconnected domains were also observed in 2D bicomponent films.

Finally, the occurrence of chemical reactions specified in Scheme 1 and further described in Fig. 6 for the TMSC/CTA 5 : 1 bicomponent fibre mats was confirmed with ATR-FTIR (Fig. 7). Because of the blend ratio used for these fibre mats, 5 : 1, the TMSC contribution was dominant. In the untreated fibre mats, characteristic peaks from CTA and TMSC were present. There was also a slight contribution from O–H stretching as expected, as both TMSC and CTA contained free OH groups (not all of the three hydroxyl groups per each anhydroglucose unit along the polymer chain were substituted). The DS of TMSC was *ca.* 2.8 and in commercial CTA there are always some units left where the DS does not reach the maximum DS of 3 (degree of acetylation 43–49%). TMSC conversion led to the fading out of the peaks characteristic for TMSC and the emergence of a notable O–H stretching peak (corresponding sample in Fig. 6: Cellulose*/CTA). Consecutive TMSC and CTA conversions to cellulose ("Cellulose/Cellulose*" fibres) were noted from the disappearance of the characteristic peaks deriving both from trimethylsilyl or acetate groups respectively and an increase in

O–H stretching contribution. After these consecutive conversions, the Cellulose/Cellulose* fibre network spectrum corresponded to that of pure cellulose. After sequential TMSC conversion and CTA dissolution ("Cellulose/*" fibres), the CTA contribution in the spectrum was still significant. It was hypothesised that CTA was surrounded by a cellulose layer (formerly TMSC), preventing chloroform diffusion and thus dissolution (Scheme 2). This hypothesis is based on the WCA measurements and is supported by these IR results.

Selective CTA conversion was observed to be effective (Fig. 7). However, when sequential CTA and TMSC conversions were executed ("Cellulose*/Cellulose" fibres), the bicomponent fibre conversion to cellulose seemed incomplete. Likewise, the characteristic peaks of the dissolved component did not disappear after successive CTA conversion and the selective dissolution of TMSC (*/*Cellulose). The TMSC contribution was still clearly visible in the spectra. This was also hypothesised to derive from the division of the components in the fibre: in addition to forming



Scheme 2 Schematic illustration indicating the hypothesised conceivable polymer distribution in a sliced bicomponent electrospun fibre. The effect of the blend ratio and pores are excluded from the illustration for clarity. TMSC and CTA are indicated in black and grey colour, respectively. The dimensions and shapes of the domains are not drawn to scale and they are used here for illustration purposes only.

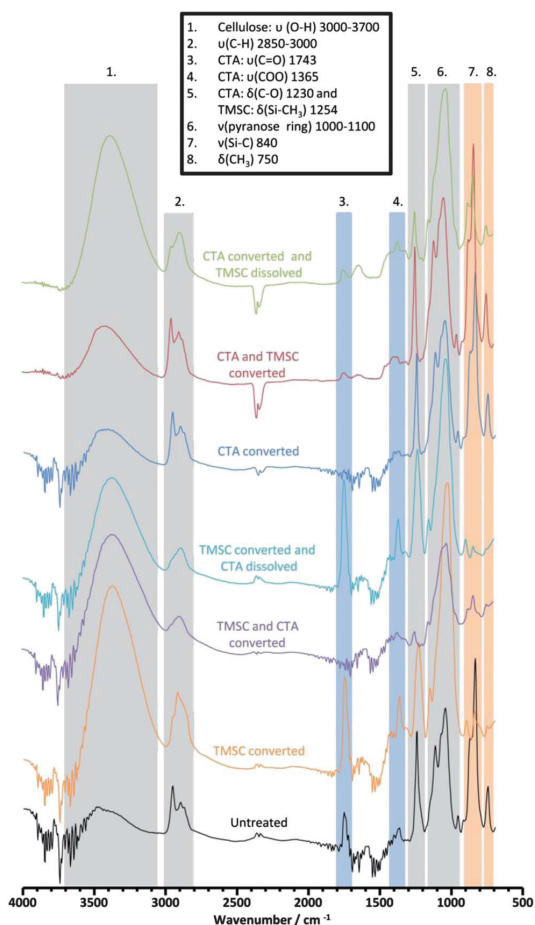


Fig. 7 ATR-FTIR spectra for the modified TMSC/CTA 5 : 1 fibre mats. The characteristic peaks for TMSC, CTA and cellulose are highlighted and explained in the legend.

an overlayer on the fibres, TMSC was speculated to be embedded inside the cellulose (formerly CTA) matrix (see Scheme 2). The diffusion of the HCl inside the cellulose matrix was hindered inhibiting the conversion and the same seemed to apply to chloroform in the case of successive CTA conversion and TMSC dissolution.

To confirm the presented hypotheses, additional characterization would provide important information on the underlying chemical basis for the behaviour of these fibres. These analyses could consist of, *e.g.*, mercury porosimetry or confocal microscopy (to determine the size of macroscopic pores between the fibres, *i.e.*, roughness in the larger length scale), extensive AFM imaging (to characterize the roughness of single fibres), a subsequent XPS analysis taking into account the roughness values (to reliably determine the surface chemical composition), and elemental analysis (to accurately quantify the remnants of TMSC and CTA that have not been regenerated and/or removed).

After comparing the obtained fibre morphologies to those of flat, solid films prepared from the same bicomponent system, some resemblances but also some differences were noted. Differences in the techniques used to produce the respective materials are obviously important. Analogous to the 2D bicomponent films, increasing the amount of CTA in the blend enhanced the pore growth in the fibres. Also, both films and fibres were hypothesized to be coated with a thin TMSC layer. As an overall summary, it can be stated that the porous film morphologies could be reproduced on 3D bicomponent fibre networks.

Conclusions

Unique morphologies from the spin coated bicomponent 2D ultrathin films of the hydrophobised cellulose derivatives were reproduced on 3D micron scale electrospun fibre networks. SEM revealed diverse fibre mat morphologies dependent on the blend ratio: electrospinning of CTA led to smooth micron and submicron fibres, TMSC to non-continuous micron fibres with shallow dints, TMSC/CTA 5 : 1 to flat micron fibres with regular pore arrays, TMSC/CTA 1 : 1 to wrinkled micron fibres decorated with shallow dints and occasional larger pores and TMSC/CTA 1 : 5 to flat micron fibres with ellipsoidal pore structure. The bicomponent fibre mats were ultra-hydrophobic (high water contact angle, >136 degrees) with high contact angle hysteresis (>50 degrees) which likely indicates Wenzel-type wetting surfaces. Strong adhesion between water and the fibre mats were observed: the water droplet remained pinned to the sample even when it was tilted 180 degrees. Specific chemical tailoring of the fibres with selective gas phase reagents and selective solvents was also demonstrated, circumventing the cumbersome reaction paths which are normally required to modify cellulosic materials. When cellulose derivatives were regenerated to cellulose, chemical and adsorption properties of the fibre networks could be tuned without significantly changing the network morphology. Potentially, this work gives insight to the design of novel materials for applications, such as filtration or controlled release. The route from 2D to 3D morphologies presents a conceptually fresh approach. Together with the possibility of large scale, cost-effective fibre production capability of electrospinning, the

proposed systems are envisioned as an attractive platform for new materials.

Acknowledgements

This work was performed as a part of LignoCell project and was financially supported by the Finnish Funding Agency for Technology and Innovation (TEKES) and Academy of Finland *via* Graduate school for biomass conversion (BIOREGS). Kati Vilonen (Aalto University) is thanked for performing the N₂ adsorption measurements, Chuck Mooney (North Carolina State University) for SEM measurements and Hannes Orelma (Aalto University) for confocal microscopy measurements. EK acknowledges Academy of Finland (no. 129068) for financial support.

References

- 1 J. Zeleny, *Phys. Rev.*, 1914, **3**, 69–91.
- 2 A. Formhals and R. Schreiber-Gastell, *Process and apparatus for preparing artificial threads*, 1934.
- 3 J. Doshi and D. H. Reneker, *J. Electrostat.*, 1995, **35**, 151–160.
- 4 D. H. Reneker and I. Chun, *Nanotechnology*, 1996, **7**, 216–223.
- 5 A. Greiner and J. H. Wendorff, *Angew. Chem., Int. Ed.*, 2007, **46**, 5670–5703.
- 6 S. Ramakrishna, K. Fujihara, W. Teo, T. Yong, Z. Ma and R. Ramaseshan, *Mater. Today*, 2006, **9**, 40–50.
- 7 S. Ramakrishna, R. Jose, P. Archana, A. Nair, R. Balamurugan, J. Venugopal and W. Teo, *J. Mater. Sci.*, 2010, **45**, 6283–6312.
- 8 S. Megelski, J. S. Stephens, D. B. Chase and J. F. Rabolt, *Macromolecules*, 2002, **35**, 8456–8466.
- 9 M. Bognitzki, W. Czado, T. Frese, A. Schaper, M. Hellwig, M. Steinhart, A. Greiner and J. H. Wendorff, *Adv. Mater.*, 2001, **13**, 70–72.
- 10 J. T. McCann, M. Marquez and Y. Xia, *J. Am. Chem. Soc.*, 2006, **128**, 1436–1437.
- 11 D. Li and Y. Xia, *Nano Lett.*, 2004, **4**, 933–938.
- 12 M. Bognitzki, T. Frese, M. Steinhart, A. Greiner, J. H. Wendorff, A. Schaper and M. Hellwig, *Polym. Eng. Sci.*, 2001, **41**, 982–989.
- 13 L. Taajamaa, O. J. Rojas, J. Laine and E. Kontturi, *Soft Matter*, 2011, **7**, 10386–10394.
- 14 J. D. Schiffman and C. L. Schauer, *Polym. Rev.*, 2008, **48**, 317–352.
- 15 D. Klemm, F. Kramer, S. Moritz, T. Lindström, M. Ankerfors, D. Gray and A. Dorris, *Angew. Chem., Int. Ed.*, 2011, **50**, 5438–5466.
- 16 M. W. Frey, *Polym. Rev.*, 2008, **48**, 378–391.
- 17 C. Kim, M. W. Frey, M. Marquez and Y. L. Joo, *J. Polym. Sci., Part B: Polym. Phys.*, 2005, **43**, 1673–1683.
- 18 P. Kulpinski, *J. Appl. Polym. Sci.*, 2005, **98**, 1855–1859.
- 19 K. Ohkawa, S. Hayashi, A. Nishida, H. Yamamoto and J. Ducreux, *Text. Res. J.*, 2009, **79**, 1396–1401.
- 20 S. Quan, S. Kang and I. Chin, *Cellulose*, 2010, **17**, 223–230.
- 21 E. Kontturi, P. C. Thuenen and J. W. Niemantsverdriet, *Langmuir*, 2003, **19**, 5735–5741.
- 22 W. Kasai and T. Kondo, *Macromol. Biosci.*, 2004, **4**, 17–21.
- 23 T. Abitbol and D. Gray, *Chem. Mater.*, 2007, **19**, 4270–4276.
- 24 D. Klemm, B. Heublein, H.-P. Fink and A. Bohn, *Angew. Chem., Int. Ed.*, 2005, **44**, 3358.
- 25 I. Filpponen, E. Kontturi, S. Nummelin, H. Rosilo, E. Kolehmainen, O. Ikkala and J. Laine, *Biomacromolecules*, 2012, **13**, 736.
- 26 H. Qi, X. Sui, J. Yuan, Y. Wei and L. Zhang, *Macromol. Mater. Eng.*, 2010, **295**, 695–700.
- 27 M. M. Hohman, M. Shin, G. Rutledge and M. P. Brenner, *Phys. Fluids*, 2001, **13**, 2201–2220.
- 28 U. H. F. Bunz, *Adv. Mater.*, 2006, **18**, 973–989.
- 29 C. L. Casper, J. S. Stephens, N. G. Tassi, D. B. Chase and J. F. Rabolt, *Macromolecules*, 2004, **37**, 573–578.
- 30 E. S. Medeiros, L. H. C. Mattoso, R. D. Offeman, D. F. Wood and W. J. Orts, *Can. J. Chem.*, 2008, **86**, 590–599.
- 31 S. O. Han, W. K. Son, J. H. Youk, T. S. Lee and W. H. Park, *Mater. Lett.*, 2005, **59**, 2998–3001.

- 32 C. Aulin, J. Netrval, L. Wagberg and T. Lindstrom, *Soft Matter*, 2010, **6**, 3298–3305.
- 33 M. Paakko, J. Vapaavuori, R. Silvennoinen, H. Kosonen, M. Ankerfors, T. Lindstrom, L. A. Berglund and O. Ikkala, *Soft Matter*, 2008, **4**, 2492–2499.
- 34 H. Sehaqui, Q. Zhou, O. Ikkala and L. A. Berglund, *Biomacromolecules*, 2011, **12**, 3638–3644.
- 35 M. Bognitzki, T. Frese, J. H. Wendorff and A. Greiner, *Book of Abstracts, 219th ACS National Meeting*, San Francisco, CA, March 26–30, 2000, PMSE-173.
- 36 R. N. Wenzel, *Ind. Eng. Chem.*, 1936, **28**, 988–994.
- 37 J. T. Korhonen, M. Kettunen, R. H. A. Ras and O. Ikkala, *ACS Appl. Mater. Interfaces*, 2011, **3**, 1813–1816.
- 38 L. Gao and T. J. McCarthy, *Langmuir*, 2006, **22**, 6234–6237.
- 39 L. Gao and T. J. McCarthy, *Langmuir*, 2007, **23**, 3762–3765.
- 40 L. Gao and T. J. McCarthy, *Langmuir*, 2009, **25**, 7249–7255.
- 41 A. Marmur and E. Bittoun, *Langmuir*, 2009, **25**, 1277–1281.
- 42 T. S. Meiron, A. Marmur and I. S. Saguy, *J. Colloid Interface Sci.*, 2004, **274**, 637–644.
- 43 P. G. de Gennes, *Rev. Mod. Phys.*, 1985, **57**, 827–863.
- 44 K.-H. Cho and L.-J. Chen, *Nanotechnology*, 2011, **22**, 445706–445720.
- 45 C. W. Extrand, *Langmuir*, 2004, **20**, 4017–4021.
- 46 T. Onda, S. Shibuichi, N. Satoh and K. Tsujii, *Langmuir*, 1996, **12**, 2125–2127.
- 47 P. Roach, N. J. Shirtcliffe and M. I. Newton, *Soft Matter*, 2008, **4**, 224–240.
- 48 A. B. Cassie and S. Baxter, *Trans. Faraday Soc.*, 1944, **40**, 546–551.
- 49 S. Wang and L. Jiang, *Adv. Mater.*, 2007, **19**, 3423–3424.
- 50 A. Marmur, *Langmuir*, 2003, **19**, 8343–8348.
- 51 D. Quéré, A. Lafuma and J. Bico, *Nanotechnology*, 2003, **14**, 1109.
- 52 G. McHale, N. J. Shirtcliffe and M. I. Newton, *Langmuir*, 2004, **20**, 10146–10149.
- 53 L. Feng, Y. Zhang, J. Xi, Y. Zhu, N. Wang, F. Xia and L. Jiang, *Langmuir*, 2008, **24**, 4114–4119.
- 54 H. Jin, M. Kettunen, A. Laiho, H. Pynnonen, J. Paltakari, A. Marmur, O. Ikkala and R. H. A. Ras, *Langmuir*, 2011, **27**, 1930–1934.
- 55 B. Balu, V. Breedveld and D. W. Hess, *Langmuir*, 2008, **24**, 4785–4790.
- 56 T. Pisuchpen, N. Chaim-ngoen, N. Intasanta, P. Supaphol and V. P. Hoven, *Langmuir*, 2011, **27**, 3654–3661.
- 57 K. Uchida, N. Nishikawa, N. Izumi, S. Yamazoe, H. Mayama, Y. Kojima, S. Yokojima, S. Nakamura, K. Tsujii and M. Irie, *Angew. Chem., Int. Ed.*, 2010, **49**, 5942–5944.
- 58 D. Wang, Y. Liu, X. Liu, F. Zhou, W. Liu and Q. Xue, *Chem. Commun.*, 2009, 7018–7020.
- 59 Z. Cheng, L. Feng and L. Jiang, *Adv. Funct. Mater.*, 2008, **18**, 3219–3225.
- 60 Z. Guo and W. Liu, *Appl. Phys. Lett.*, 2007, **90**, 223111.
- 61 E. Bormashenko, T. Stein, R. Pogreb and D. Aurbach, *J. Phys. Chem. C*, 2009, **113**, 5568–5572.
- 62 S. E. Harton, J. Luening, H. Betz and H. Ade, *Macromolecules*, 2006, **39**, 7729–7733.